HHS Public Access

Author manuscript

Biomaterials. Author manuscript; available in PMC 2022 February 01.

Published in final edited form as:

Biomaterials. 2021 February ; 269: 120651. doi:10.1016/j.biomaterials.2021.120651.

Mechanical, compositional and morphological characterisation of the human male urethra for the development of a biomimetic tissue engineered urethral scaffold

Eoghan M. Cunnane[1,2], **Niall F. Davis**[2], **Connor V. Cunnane**[3], **Katherine L. Lorentz**[1], **Alan J. Ryan**[2], **Jochen Hess**[4], **Justin S. Weinbaum**[1,5,6], **Michael T. Walsh**[3], **Fergal J. O'Brien**[2,7,8], **David A. Vorp**[1,5,9,10,11]

[1]Department of Bioengineering, University of Pittsburgh, Pittsburgh, PA 15213, US. [2]Tissue Engineering Research Group, Dept. of Anatomy, Royal College of Surgeons in Ireland (RCSI), Dublin, D02 YN77, Ireland. [3]School of Engineering, Health Research Institute and the Bernal Institute, University of Limerick, Limerick, V94 T9PX, Ireland. [4]Department of Urology, University Hospital Essen, University Duisburg-Essen, 45147 Essen, Germany. [5]McGowan Institute for Regenerative Medicine, University of Pittsburgh, Pittsburgh, PA 15219, United States. [6]Department of Pathology, University of Pittsburgh, Pittsburgh, PA 15213, US. [7]Trinity Centre for Biomedical Engineering, Trinity College Dublin (TCD), Dublin, D02 R590, Ireland. [8]Advanced Materials and Bioengineering Research Centre (AMBER), RCSI and TCD, Dublin, D02 R590, Ireland. [9]Department of Surgery, University of Pittsburgh, Pittsburgh, PA 15213, US. [10]Department of Cardiothoracic Surgery, University of Pittsburgh, Pittsburgh, PA 15213, United States. [11]Department of Chemical and Petroleum Engineering, University of Pittsburgh, PA 15213, United States.

Abstract

This study addresses a crucial gap in the literature by characterising the relationship between urethral tissue mechanics, composition and gross structure. We then utilise these data to develop a

Address correspondence to: David A. Vorp, Ph.D., John A. Swanson Professor of Bioengineering, Professor of Cardiothoracic Surgery, Surgery, Chemical and Petroleum Engineering, and the Clinical and Translational Sciences Institute, University of Pittsburgh, 300 Technology Drive, Suite 300, Center for Bioengineering, Pittsburgh, PA 15219, Phone: 412-624-5317, FAX: 412-383-8788 (shared), vorp@pitt.edu.

[11]Author Credit Statement

EC: Conceptualization, Methodology, Validation, Formal Analysis, Investigation, Data Curation, Writing - Original Draft, Visualisation, Project Administration, Funding Acquisition. **ND**: Conceptualization, Resources, Writing - Review & Editing, Project Administration. **CC** and **KL**: Investigation, Writing - Original Draft, Visualisation. **AR**: Conceptualization, Methodology. **JH**: Conceptualization, Methodology, Writing - Review & Editing. **JW**: Writing - Review & Editing, Supervision. **MW**, **FO'B**, **DV**: Conceptualization, Resources, Writing - Review & Editing, Supervision, Project Administration, Funding Acquisition.

[9]Conflict of Interests

The authors do not have any financial or commercial conflict of interests to declare.

Declaration of interests

The authors declare that they have no known competing financial interests or personal relationships that could have appeared to influence the work reported in this paper.

biomimetic urethral scaffold with physical properties that more accurately mimic the native tissue than existing gold standard scaffolds; small intestinal submucosa (SIS) and urinary bladder matrix (UBM).

Nine human urethra samples were mechanically characterised using pressure-diameter and uniaxial extension testing. The composition and gross structure of the tissue was determined using immunohistological staining. A pressure stiffening response is observed during the application of intraluminal pressure. The elastic and viscous tissue responses to extension are free of regional or directional variance. The elastin and collagen content of the tissue correlates significantly with tissue mechanics.

Building on these data, a biomimetic urethral scaffold was fabricated from collagen and elastin in a ratio that mimics the composition of the native tissue. The resultant scaffold is comprised of a dense inner layer and a porous outer layer that structurally mimic the submucosa and corpus spongiosum layers of the native tissue, respectively. The porous outer layer facilitated more uniform cell infiltration relative to SIS and UBM when implanted subcutaneously ($p < 0.05$). The mechanical properties of the biomimetic scaffold better mimic the native tissue compared to SIS and UBM.

The tissue characterisation data presented herein paves the way for the development of biomimetic urethral grafts, and the novel scaffold we develop demonstrates positive findings that warrant further *in vivo* evaluation.

Keywords

Urethral tissue; tissue characterisation; mechanical properties; collagen-elastin scaffold; subcutaneous implant

1 Introduction

The human urethra is a complex tubular organ that allows urine to drain from the urinary bladder. It is comprised of smooth and striated muscle that is contained within a connective tissue matrix composed primarily of collagen and elastin [1]. The muscle component functions as a sphincter by producing closure pressure to maintain urinary continence, and the extracellular connective tissue matrix plays a passive role in preventing the urethra from over distending during increases in intraluminal urethral pressure and distension [2].

Urethral trauma is a frequent and costly event that can be caused by injury, inflammation, ischaemic stricture, congenital defect or malignancy [3]. The most recent estimates place the cost of managing urethral trauma at almost $200M [4] per annum in the US, with the annual cost of urethral repair alone at over $10M [5,6]. Urethral trauma is often repaired using a flap or vascularised graft. However, autologous grafts are difficult to harvest, have limited availability, increase procedural costs and are associated with donor site morbidity [5,7]. Tissue engineered urethral scaffolds are not subject to such limitations and present as a viable treatment option in certain clinical cases. However, despite numerous preclinical and clinical trials [8], urethral scaffolds made of the ‘gold standard’ tissue engineered materials; small intestinal submucosa (SIS) or urinary bladder matrix (UBM), frequently fail in cases

of long strictures (i.e. >2 cm), tubular grafting, grafting in unhealthy residual urethral beds or grafting of penile strictures [9].

The poor clinical outcomes associated with SIS and UBM in certain clinical indications can be linked to the disparity that exists between the scaffold material and the native tissue. SIS and UBM are fabricated from densely packed laminates of decellularised tissue and therefore do not mimic the composition, structure or mechanical properties of the native tissue. Developing a urethral scaffold that is more mimetic of the native tissue would enable improved physiological function, provide more appropriate biomechanical cues to endogenous cells, and allow for improved integration of the scaffold by the native host tissue, thereby improving clinical outcomes [10,11].

Data characterising the relationship between the mechanics, composition and structure of human urethral tissue is therefore paramount to providing an accurate baseline for biomimetic tissue engineered urethral scaffolds. However, such data has not yet been made available to the scientific community. Therefore, a crucial gap in the current literature exists that restricts the development of biomimetic tissue engineered scaffolds for urethral grafting.

For the first time, this study comprehensively characterises the baseline mechanical properties of human male anterior urethral tissue and relates these properties to the composition and gross morphology of the tissue. Our results reveal that urethral tissue exhibits viscoelastic mechanical properties, with no directional or regional variance, that correlate with elastin and collagen content. These novel data are used to inform the design of the first biomimetic tissue engineered urethral scaffold. Through a combination of *in vitro* and *in vivo* tests, our novel bilayered scaffold is shown to be more mimetic of the native urethral tissue in terms of mechanical properties, composition and gross structure compared to existing gold standard tissue engineered materials, and also exhibits improved cellular infiltration.

2 Methods

2.1 Acquisition of Donor Tissue

Following hospital ethical research committee approval, human anterior urethras were obtained from 9 consenting male patients undergoing male to female gender reassignment surgery at the University Hospital Essen, Essen, Germany. The mean age of the patients was 40±13.13 years (Range: 18 to 58 years). Samples included the anterior portion of the urethra which can be further divided into the bulbar portion of the urethra at the proximal end, penile (pendulous) urethra and the urethra bearing potion of the glans at the distal end. The corpus spongiosum, a mass of spongy tissue that surrounds the anterior urethra, was included with the samples. The urethra bearing potion of the glans was removed prior to testing to facilitate for mounting of the samples in the pressure-diameter testing apparatus.

Samples were stored at −20°C within 2 h of excision. This method of storage was employed as it has been previously demonstrated to have no significant effects on biological soft tissue mechanical properties once the tissue is unfrozen [12,13]. Prior to testing, samples were defrosted overnight at 4°C and subsequently immersed in deionised distilled water (ddH_2O)

at 37°C to equilibrate the tissue back to physiological temperature. Samples were maintained at their *in vivo* length by tethering the urethra to a urinary catheter during surgical excision. Prior to mechanical testing, the *in vivo* length and external diameter of samples were measured using Vernier callipers. Measurements were confirmed using a non-contact photography method. The mean *in vivo* length of the samples was 147.44±13.97 mm (Range: 122.96 to 167.76 mm). Samples were then marked with acrylic paint at points 5 cm from each end. This distance was measured to allow for restoration of samples to their *in vivo* length and to ensure proper alignment of the samples in the pressure-diameter apparatus. Samples were then detached from the urinary catheter and allowed to retract for 3 min prior to measuring *ex vivo* length. The mean ratio of *in vivo* length to *ex vivo* length was 1.29±0.12 (Range: 1.11 to 1.46).

2.2 Pressure-Diameter Testing

Samples were mounted in a pressure-diameter testing apparatus similar to that previously reported [14,15] and shown in Figure 1A. Physiological humidity and temperature were achieved during testing by submersing the samples in a ddH_2O bath maintained at 37°C. The elastic response of the samples was characterised by subjecting the samples to dynamic Intraluminal pressure using a 100 mL syringe (BD, USA) and a syringe pump (Pump Systems Inc., USA, Model: NE-1000). The viscoelastic response of the samples was characterised by subjecting the samples to a static pressure head of adjustable height. The resulting pressure was monitored using a calibrated 1 bar pressure transducer (Sensortecknic, USA). The corresponding change in sample diameter was monitored using a video extensometer (Messphysik, Austria), Figure 1A.

Each end of the sample was mounted on stainless steel tubular mounts (outer diameter = 6.5 mm, inner diameter = 5 mm) lined with 60 grit sandpaper and secured with wire hose clips of internal diameter ranging from 9 to 13 mm. Samples were then aligned and restored to their *in vivo* length. The system was purged of air via a release valve located distally to the distal sample mount. The external diameter of the sample was measured with Vernier callipers and a non-contact photography method. This was used as the reference diameter for the video extensometer. Samples were inspected for leaks prior to completely filling the ddH_2O bath.

Samples were preconditioned by applying 9 cycles of intraluminal pressure that each ranged from 0 to 10 kPa at an infusion rate of 50 mL/min. A strain-softening effect was observed during the application of repeat intraluminal loading to 10 kPa, Supplementary Figure S1. Samples were characterised dynamically by performing a further inflation cycle to 10 kPa immediately after preconditioning to examine the elastic response of the tissue to intraluminal pressure. The samples were then inflated to 10 kPa of static intraluminal pressure in increments of 1 kPa using an appropriate pressure head. The pressure was maintained for 300 seconds at each increment to examine the creep of the samples and characterise their viscoelastic behaviour. The upper pressure limit of 10 kPa was chosen to mimic the upper limit of intra-urethral pressure during micturition [16] and also to avoid trauma to the urethral structure during testing as porcine urethras have previously been shown to rupture at intraluminal pressures exceeding 50 kPa [17].

The resulting pressure-diameter data were used to compute tissue compliance over linear portions of the curve. The following pressure ranges were characterised: 0 to 3 kPa (low), 3 to 5 kPa (middle), and 6 to 10 kPa (high). Multiple ranges were taken to characterise the linear portions of the nonlinear pressure-diameter curve. Compliance is calculated as:

$$C = \frac{D_{max} - D_{min}}{D_{min}} \times (P_{max} - P_{min})^{-1}$$

where D_{max} and D_{min} are the sample diameter at the maximum pressure, P_{max}, and minimum pressure, P_{min}, within the relevant pressure range.

Beta stiffness, a dimensionless parameter that describes the full range of the nonlinear pressure-diameter response, was also calculated as:

$$\beta = \frac{\ln\left(\frac{P}{P_S}\right)}{\left(\frac{D}{D_S} - 1\right)}$$

where P_s and D_s are the standard pressure and corresponding standard diameter, respectively. P_s and D_s were taken at 5 kPa, as this is the midpoint of the investigated pressure range.

The incremental elastic modulus, E_{inc}, characterises tissue stiffness by accounting for the changes in tubular geometry induced by incremental increases in pressure. It provides a modulus that represents both the radial and circumferential directions at a given increment. It is defined as:

$$E_{inc} = \frac{\Delta P_I}{\Delta R_o}\left(\frac{2R_i^2 R_o}{R_o^2 - R_i^2}\right) + \left(\frac{2P_I R_o^2}{R_o^2 - R_i^2}\right)$$

where R_i, R_o and P_I are the inner and outer radius and the total pressure at the beginning of each increment (1 kPa), respectively.

To determine the thickness of each sample, a central tubular section was removed for histological analysis. The thickness was measured from the resulting stained images at 0, 90, 180 and 270° to a reference axis originating from the lumen centre, using ImageJ [18], and an average value was calculated to represent sample thickness. This method accounts for the eccentricity of the sample lumens. The mean thickness value recorded using this method was 3.41±0.59 mm (Range=2.65 to 4.44 mm).

It is assumed that the tissue is incompressible and that length changes do not occur during testing. Therefore, it can be assumed that the cross-sectional area does not change, regardless of increases in intraluminal pressures. The following relationship can therefore be employed:

$$\pi\left(R_o^2 - R_i^2\right)_{P_x} = \pi\left(R_o^2 - R_i^2\right)_{P_o}$$

where, $\left(R_o^2 - R_i^2\right)_{P_x}$ refers to the outer and inner radii at any applied pressure (P_x), and $\left(R_o^2 - R_i^2\right)_{P_o}$ refers to the outer and inner radii measured at 0 kPa (P_o).

Therefore, the following equation can be used to calculate R_{ipx}:

$$R_{i}P_x = \sqrt{R_o^2 P_x - R_o^2 P_o + R_i^2 P_o}$$

2.3 Extension Testing

Samples were sectioned longitudinally into 20 mm wide rings that represent the distal and proximal regions of the penile and bulbar urethra, Figure 2A. This resulted in 3 to 4 rings per urethra (n = 31 total). The rings were incised longitudinally and the thickness of each flat section was measured using Vernier callipers and a noncontact photography method. The average number of individual thickness measurements for each section was 8.2 (Range: 6 to 9) and the mean recorded value was 4.44±0.64 mm (Range: 3.1 to 5.67 mm). Sections were mechanically characterised sequentially under circumferential and then longitudinal extension in a ddH_2O bath maintained at 37°C using a dedicated device designed for the extension of biological soft tissues (CellScale, Canada). This allowed for the regional and directional mechanical properties of the urethral tissue to be determined. As the gauge length did not exceed 5 mm in any section (Circumferential: Mean = 4.52±0.42 mm, Longitudinal: Mean = 4.31±0.42 mm, Range: 4 to 5), the sections are considered to be in planar tension as the width to length ratio is greater than 4:1 [19]. Planar tension testing is advantageous compared to pure tension testing as it provides an enlarged contact area between the clamps and the tissue which reduces slippage [20].

The sections were firstly orientated in the circumferential direction and the edges were placed in clamps that were lined with foam-backed sandpaper. A torque of 7.5 cN.m was applied to a single centrally positioned bolt on the tissue clamps. The clamped sections were allowed to equilibrate in the water bath for 3 minutes prior to testing. The elastic mechanical properties of the sections were characterised by stretching the tissue to a preload of 0.01 N and then subjecting it to 10 cycles of extension to a stretch equal to 2.5 times the sample gauge length at a displacement rate of 45 mm/min which equates to a rate of 15 % of the section gauge length per second, Figure 2B. This rate was chosen as it was shown to minimise viscous phenomena (i.e., reduce hysteresis) and prevent the dynamic effects that arise at higher rates (i.e., unloading stress exceeding corresponding loading stress) during preliminary testing [21,22]. Ten cycles were performed to minimise the stress softening effect displayed by soft biological tissues [23]. The fifth cycle was employed to characterise the elastic response of the tissue to extension, as the mechanical response curve was seen to be repeatable after the fourth cycle. The extension limit of 2.5 stretch was chosen as this was the limit of stretch prior to sample slippage during preliminary testing. The absence of sample slippage was confirmed by the absence of slack in the samples following testing.

The viscous mechanical properties of the tissue were then characterised using stress relaxation and creep tests. Sections were extended to a stretch of 2.5 times the gauge length at a displacement rate of 45 mm/min and held at this stretch for 300 seconds to examine the stress relaxation response of the tissue. Sections were then unloaded and permitted to recover for 30 seconds before being extended to a load of 0.4 N and held at this load for 300 seconds to examine the creep behaviour of the tissue, Figure 2B. Sections were then reoriented and both the elastic and viscous testing was repeated in the longitudinal direction. Stress relaxation data was analysed using the following model [23]:

$$\sigma\left\{t\right\} = (1 - \gamma_1 - \gamma_2) + \gamma_1 \exp\left(\frac{-t}{\tau_1}\right) + \gamma_2 \exp\left(\frac{-t}{\tau_2}\right)$$

Creep data was analysed using Burger's four-parameter constitutive model [24]:

$$\varepsilon\left\{t\right\} = \frac{\sigma_0}{R_1} + \frac{\sigma_0}{\eta_1}t + \frac{\sigma_0}{R_2}\left[1 - exp\left(\frac{-R_2 t}{\eta_2}\right)\right]$$

2.4 Histological and Immunohistochemical Examination

Masson's trichrome and Verhoeff-Van Gieson stains were employed to histologically examine the collagen and elastin content of the urethral tissue matrix following mechanical characterisation. Small ring segments (approx. 5 mm) were cut from the middle region of the tubular urethras prior to sectioning for extension testing and fixed in their traction-free state in 10% formalin, embedded in paraffin, and then sliced into 10 μm thick segments. Immunohistochemical staining of muscle actin was also used to identify the smooth and striated muscle content of the samples. Images of the stained samples were obtained using a Nikon microscope (Eclipse, 90i) at 4x and 20x for gross and detailed imaging respectively. The composition of each sample was assessed from the histological images using a previously outlined protocol which employs ImageJ to convert collagen composition to the mean Gray value of the blue colour intensity of the Mason's Trichrome stains with respect to tissue area [25]. This protocol uses hue (121–179), saturation (20–255) and brightness (10–255) to isolate collagen and is also adapted for elastin and muscle content. Both elastin and muscle content are identified using the YUV colour space (elastin: Y=0–120, muscle: Y=0–145, both: U and V=0–255). Gross morphological characterisation of the sample cross section was also performed by examining the histological sections. Shape descriptors of the entire cross-section and the lumen were quantified using ImageJ. These descriptors include area, perimeter, maximum diameter and minimum diameter.

2.5 Scanning Electron Microscopy

An additional human urethra sample was sectioned to expose the luminal, abluminal and cross-section surfaces prior to examination using scanning electron microscopy (SEM). The samples were prepared for SEM using a previously outlined method of fixation, chemical dehydration and drying to maintain tissue structure [26]. Briefly, the tissue sections were initially cleaned in fresh phosphate buffered saline and fixed in methanol (Fisher Scientific, Product code: 10020260) for 10 min. The fixed sections were washed in ethanol prior to passing through ascending increments of ethanol (99.5% (v/v)) (Fisher Scientific, Product

code: 10644795) and ddH2O mixtures (30% ethanol up to 100% ethanol in increments of 30%, 50%, 70%, 80%, 90% and 95% ethanol) for ten minutes at each increment. The dehydrated sections were chemically dried in a hexamethyldisilazane (Sigma–Aldrich, Product code: 440191) and ethanol mixture (50:50) for 10 min prior to being transferred into 100% hexamethyldisilazane for 10 min. The sections were left in a fume hood overnight prior to gold plating at 30 mA for 120 s using an Emitech K550 (Emitech Ltd. UK). SEM imaging (Hitachi SU-70 High-Technologies Europe GmbH, Germany) was performed at an accelerating voltage of 10 kV with a magnification of either x100 or x200.

2.6 Construction of a Novel Tissue Engineered Urethral Scaffold

Scaffolds were constructed from collagen (bovine deep flexor tendon) and elastin (bovine neck ligament) to assess their suitability to act as a more biomimetic urethral scaffold compared to existing gold standard materials. These two proteins were selected as they are two of the main constituents of the urethral tissue matrix, they exhibit viscoelastic mechanical properties, and they also provide appropriate cues to native cells [27]. The tissue characterisation performed during this study revealed that the ratio of elastin to collagen in the native urethral tissue is 0.3:1 (See Section 3.3). Therefore, an elastin to collagen ratio of 0.3:1 was used to fabricate our biomimetic scaffolds, in order to mimic the native tissue. Bilayered scaffolds were fabricated with an inner desiccated film layer and an outer freeze-dried layer. The dense luminal layer is intended to prevent urine infiltration and offer a smooth surface for epithelialisation, while the outer porous layer is intended to facilitate endogenous cell infiltration upon implantation. A co-suspension of collagen and elastin was prepared in an acetic acid solution as per [27]. Briefly, 0.5% w/v type I microfibrillar collagen from bovine deep flexor tendon (Integra Life Sciences, Plainsboro, NJ) and 0.15% w/v elastin from bovine neck ligament (Sigma-Aldrich, Germany) were added to a 0.05 M acetic acid solution. The suspension was added to a mixing vessel, cooled to 4°C, and blended using an overhead blender (Ultra Turrax T18, IKA Works Inc., Wilmington, NC) at a speed of 12,000 rpm to homogenise the suspension. A vacuum chamber was then used to degas the suspension.

Dense collagen-elastin films were produced by adding 7 mL of the suspension to a 2025 mm^2 square stainless steel mould secured to a polytetrafluoroethylene plate and leaving the suspension uncovered in a fume hood for 24 h. The films were rehydrated in a 0.05 M acetic acid solution and an additional 14 mL of the suspension was added to the mould. The suspension was frozen at a cooling rate of 0.9°C/minute to a final freezing temperature of −40°C, in order to produce a porous layer with a homogenous pore structure, and then dried at 0°C for 17 h using a freeze-drier system (Advantage EL, Vir-Tis Co., Gardiner NY) [28]. The scaffolds were sterilised and crosslinked as per [29]. Briefly, the films were subjected to a treatment of 105°C for 24 h at 0.05 bar in a vacuum oven (Vacucell 22, MMM, Germany).

2.7 Characterisation of the Novel Urethral Scaffold

The mechanical properties of the bilayered scaffold were characterised using the extension tests previously outlined in Section 2.3. Briefly, samples were sectioned into 15 × 15 mm sections. The number of individual thickness measurements for each sample was 9 and the mean recorded value was 3.61±0.06 mm (Range: 3.55 to 3.7 mm). Samples were

mechanically characterised in a single orientation (n = 3) and then separate samples were characterised in the opposite orientation (n = 3). The elastic and viscous mechanical properties of the samples were characterised in the same manner as the urethral tissue with the exception of extension limit which was set to 1.5 times the sample gauge length.

The burst pressure of the dense inner layer was tested to ensure that the scaffold can withstand the physiological pressure generated during voiding (10 kPa). Tubular samples of the dense inner layer were formed by wrapping the films around a 5 mm mandrel prior to rehydration. The films were then allowed to dry overnight and rehydrated in ddH_2O prior to testing. Samples were mounted within a custom fabricated burst pressure apparatus and pressure was increased at a constant rate using a syringe pump until the sample burst. Pressure was recorded using a digital pressure manometer.

Suture retention force of the bilayered scaffold was quantified using the American National Standard Institute–Association for the Advancement of Medical Instruments (ANSI/AAMI) VP20 standards. Briefly, a 7–0 polypropylene (SURGIPRO II, Syneture) was placed through the scaffold ~2 mm from the scaffold edge. The ends of the suture were secured in the upper pneumatic clamp of a tensile testing device (Instron model 5543A) using labelling tape (Fisher Scientific) and the scaffold was secured in the lower clamp. A pre-load of 0.01 N was applied and load-displacement curves were recorded at a displacement rate of 2 mm/min until failure. Maximum load prior to suture pull-out is reported as suture retention force.

The upper, lower and cross sectional aspects of the bilayered scaffold were characterised using SEM as outlined previously in Section 2.5. Briefly, samples were gold plated and imaged at an accelerating voltage of 10 kV with a magnification of either x100 or x200. Mean pore size of the bilayered scaffold was calculated from the upper and cross-section micrographs as the mean maximum diameter of 50 pores. In all cases, the results obtained from scaffold characterisation were compared to the native tissue and also to commercially available small Intestinal submucosa (SIS; Cook, Indiana) and urinary bladder matrix (UBM; Acell, Indiana) as these are the current gold standard tissue engineered materials for urethral repair applications (as reviewed in [9]). Commercially available materials were tested in an identical manner to the bilayered scaffold material.

2.8 *In vivo* Assessment of Cell Infiltration in the Urethral Scaffold

Urethral scaffolds were implanted subcutaneously in a murine model to examine the cellular infiltration into each scaffold after 1 week. A 1 week time point was chosen as it has been previous shown to coincide with peak macrophage infiltration within tissue engineered grafts [30]. Animal procedures were performed using a protocol approved by the University of Pittsburgh Institutional Animal Care and Use Committee. Details of how the in vivo studies adhered to the ARRIVE guidelines are outlined in the Supplementary Information. Scaffolds were surgically implanted as subcutaneous implants in Lewis rats (n = 5). Briefly, 4–6 month old rats, weighing between 200 to 300 grams, were anesthetized using ketamine (30 mg/kg) and kept under sedation for the duration of the surgery using nose cone administration of isoflurane (1.5 L/min in oxygen). The dorsal skin was shaved and three separate incisions measuring approximately 2 cm were made at equidistance in the dorsal

skin. A collagen-elastin, SIS or UBM scaffold (10 mm diameter) was then placed in the incision. The dorsal skin was closed with 3–0 polyglactin sutures (McKesson, Richmond, Va). Buprenorphine hydrochloride (500 μl per rat) was administered postoperatively every 12 h for the first 72 h.

After 1 week, rats were euthanized using isoflurane and a single intracardiac injection of 10 units/kg rat of heparin/KCl. The graft and adjacent tissue were excised using a 14 mm biopsy punch. The explant was placed in a 4% paraformaldehyde solution (Sigma-Aldrich, #158127), paraffin embedded and sectioned for histological analysis. Sections were stained for the presence of macrophages using a primary antibody for CD68 (BioRad, MCA341GA) and a Cy5 secondary. Sections were then counter stained with DAPI and mounted prior to imaging with a fluorescent microscope (Nikon Digital Eclipse 90i).

2.9 Statistical Analysis

Statistical analysis was performed using GraphPad Prism 8 (GraphPad Software, San Diego, CA, USA). The normality of all variables was examined using Shapiro-Wilk tests. Significant differences were identified between groups of continuous variables using Student's t-test for normally distributed data and exact 2-tailed Mann-Whitney U tests for non-normally distributed data. Correlations between variables were assessed using 2-tailed parametric bivariate analysis. Regression analysis was performed to examine the relationship between continuous variables. A p-value of less than 0.05 is considered statistically significant.

3 Results

3.1 Pressure-Diameter Testing of Urethra Samples

Pressure-diameter testing of the urethra samples was performed to characterise the baseline mechanical properties of the tissue. Figure 1 shows the mechanical results obtained from static and dynamic pressure-diameter testing of intact human male urethras (n = 9). The results reveal a nonlinear response typical of biological tissue whereby the urethral tissue becomes stiffer at higher intraluminal pressures during both static and dynamic loading in all samples, Figures 1B and C. The stiffening effect is further evidenced by the increasing incremental modulus exhibited by each sample during both static and dynamic loading, Figures 1D and E. The pronounced viscoelastic behaviour of the tissue is evidenced in Figure 1F by the increases in stretch observed at each pressure increment when comparing static loading to dynamic loading ($p < 0.05$). However, a similar increase in incremental modulus is not observed at each pressure increment when comparing static and dynamic loading ($p > 0.05$), Figure 1G. Table 1 displays the mean Beta stiffness, compliance and incremental modulus of the samples under static and dynamic loading. The reduction in compliance across all pressure ranges ($p < 0.05$) and the increase in Beta stiffness during dynamic loading compared to static loading ($p < 0.05$) further demonstrates the pronounced viscoelastic behaviour of the tissue.

3.2 Extension Testing of Urethra Sections

Extension testing of urethra sections was performed to examine the directional and regional variance of the tissue mechanical response. Figure 2 shows the mechanical results obtained from uniaxial extension testing (n = 31). Figure 2C shows the patient averaged responses of the urethral tissue to planar tension testing in the circumferential and longitudinal direction. Differences between the directional responses are not observed at any stress level for the patient averaged mechanical responses ($p > 0.05$), Figure 2C. Furthermore, differences between directional responses to extension are not observed at any stress level for the region averaged mechanical responses ($p > 0.05$), Supplementary Figure S2. Differences between regional responses to extension are not observed during circumferential or longitudinal extension ($p > 0.05$), Figures 2D and E. A comparison of the circumferential stress calculated in the samples during the application of intraluminal pressure and the circumferential extension test results is included in the Supplementary Information.

Figure 2G–I display the stress relaxation of the samples in response to sustained extension, while Table 2 displays the parameters that define this response. **Figure 2J–L** defines the creep of the samples in response to sustained force, while Table 3 display the parameters that define this response. Differences are not observed in terms of the relaxation or creep parameters that define the response to sustained extension or stress in the circumferential or longitudinal direction ($p > 0.05$). Similarly, differences are not observed between the regions in terms of the relaxation or creep parameters for circumferential or longitudinal loading ($p > 0.05$).

3.3 Assessment of Urethral Tissue Composition

Histological staining of the urethra samples was performed to characterise the composition and morphology of the tissue, and to relate these parameters to the mechanical behaviour of the samples. Figure 3A shows histological images of elastin, muscle and collagen distribution in each sample. Figures 3B to D show selected stained samples under increased magnification. The images illustrate the inner non-porous submucosa layer adjacent to the lumen and the outer porous corpus spongiosum. Figures 3E to G illustrate the location and morphology of the structural proteins and cells. Elastin is located mainly in the submucosal and inner muscular layers, and displays a wavy fibrous conformation. Striated muscle fibres are constrained to the outer adventitial layer with smooth muscle cells located throughout the inner muscular layer. Collagen fibres are located throughout the structure with coiled, wavy collagen fibres located in organised bundles in the outer adventitial layer. Table 4 demonstrates the area and percentage area that the components occupy in each sample. On average, collagen occupies 59.02±7.21%, elastin occupies 17.05±5.21% and muscle occupies 23.93±5.2% of the urethra cross-section. The ratio of elastin to collagen content (0.3±0.11) is also included in Table 4 as it was subsequently utilised in the fabrication of a novel biomimetic urethral scaffold. The colour intensity per tissue area is employed to examine the relationship between composition and tissue mechanics as previously outlined for tissue extracellular matrix characterisation [25].

Figures 3H to K show linear regression of the significant relationships identified between tissue composition and tissue mechanics as characterised by the application of static

intraluminal pressure. Positive relationships exist between elastin content and compliance in the low pressure range ($p < 0.05$), and between collagen content and Beta stiffness ($p < 0.05$) and incremental modulus in the mid ($p < 0.05$) and high ($p < 0.05$) pressure ranges. A significant relationship is not present between tissue mechanics and muscle content. This could be attributed to the absence of muscle activators in the ddH_2O bath [14,15]. However, axial pre-stretch of the samples prior to de-tethering demonstrates positive relationships with elastin ($p < 0.05$) and muscle content ($p < 0.005$). Furthermore, axial pre-stretch displays a negative relationship with age ($p < 0.05$). Pearson's correlation coefficients relating tissue composition and mechanics are included in Supplementary Table S1.

3.4 Assessment of Urethral Tissue Gross Morphology

Figure 4 shows linear regression of the relationships identified between urethra cross-section or lumen shape descriptors and tissue mechanics as characterised by the application of static intraluminal pressure. Maximum sample diameter correlates with Beta Stiffness ($p < 0.05$), compliance in the high pressure range ($p < 0.05$), overall incremental modulus ($p < 0.05$) and incremental modulus in the mid ($p < 0.05$) and high ($p < 0.01$) pressure ranges. Furthermore, maximum sample diameter also correlates with collagen content ($p < 0.05$). The perimeter of the lumen correlates with Beta stiffness ($p < 0.05$), overall incremental modulus ($p < 0.05$) and compliance/incremental modulus in the mid ($p < 0.05$) and high ($p < 0.05$) pressure ranges. Supplementary Table S2 and S3 show the Pearson's correlation coefficients relating overall and lumen shape descriptors with tissue mechanics and collagen content. Supplementary Table S4 shows the overall and lumen geometrical dimensions of the human urethral samples characterised in this study.

3.5 Tissue Engineered Urethral Scaffold Characterisation

The mechanical properties and structure of the bilayered scaffold were characterised and compared to the native tissue and gold standard tissue engineering scaffolds; SIS and UBM. Figure 5 shows the results of mechanically and structurally characterising the native tissue and tissue engineered scaffolds. The mechanical properties of the tissue engineered materials and the native tissue are compared by calculating the modulus of each material in both the low and high stretch regions to account for the nonlinear mechanical response of the materials to extension as outlined previously [31]. The SIS and UBM exhibit moduli 284.11 and 783.1 times higher than the native tissue in the low stretch region ($p \leq 0.0001$), respectively, Figure 5B. Furthermore, the SIS and UBM exhibit moduli 413.6 and 585.2 times higher than the native tissue stiffness in the high stretch region ($p < 0.0001$), Figure 5C. However, the bilayered scaffold exhibits a modulus only 11.79 times higher than the native tissue in the low stretch region ($p > 0.05$) and 3.98 times higher in the high stretch region ($p > 0.05$), Figure 5B and C. All constructs exhibit similar creep behaviour, which is reduced compared to the native tissue Figure 5. However, the bilayered scaffold exhibits increased stress relaxation compared to the native tissue, SIS and UBM, Figure 5E.

Figure 5F shows the upper, lower and cross-sectional faces of the native tissue and tissue engineered scaffolds. The abluminal surface of the native tissue appears porous while the luminal surface appears as a non-porous barrier. The cross-section appears populated with collapsed pores that likely resembled the porous corpus spongiosum visible in histological

sections (see Figure 3B to D), prior to deformation of the structure due to tissue preparation for SEM. The structure of the bilayered scaffold is porous on the upper face and cross-section, while the SIS and UBM are formed from dense laminated sheets that do not exhibit a porous structure on either the upper face or cross-section. The lower face of all three scaffolds appears as a non-porous barrier, Figure 5F. The mean pore size of the bilayered scaffold is 95.28±21.25 μm and 147.02±39.75 μm on the upper face and cross-section, respectively. No pores were visible on the lower face. The burst strength of the tubular inner layer of the bilayered scaffold was 40.11±5.93 kPa, a value that is 4 times higher than the maximum recorded value for intra-urethral pressure during voiding [16]. The suture retention force of the bilayered scaffold was 602.41±71.27 mN, a value previously shown to be sufficient for anchorage of tissue engineered scaffolds to tubular soft tissues [32].

3.6 In vivo Assessment of Cellular Infiltration in the Urethral Scaffolds

Urethral scaffolds were implanted subcutaneously in a murine model to examine the cellular infiltration that occurs in each scaffold after 1 week. Figure 6 displays qualitative and quantitative analysis of the explanted urethral scaffolds. Figure 6B to D shows immunofluorescent staining of the explanted scaffolds. Figure 6E reveals that the bilayered scaffold facilitates increased cell infiltration relative to controls ($p < 0.05$). However, cellular density of the bilayered scaffold is not increased ($p > 0.05$), Figure 6F. There is no difference in the fraction of CD68 positive cells that the 3 scaffold types attract ($p > 0.05$), Figure 6G. It can be observed that cellular infiltration of the SIS and UBM scaffolds is largely restricted to the lateral edges of the scaffolds, Figure 6B to C. This contrasts with the cellular infiltration observed in the bilayered scaffold whereby cells are not restricted to the lateral edges but are also able to penetrate the upper face of the scaffold resulting in more complete and even cell infiltration, Figure 6B. This point is highlighted by examining an area of interest that is 0.1 mm^2 at a depth of 100 μm from the upper face (inset boxes in Figures 6B to D). Figure 6H demonstrates that there is dramatically increased cellular infiltration within this area of interest in the bilayered scaffold compared to SIS and UBM ($p < 0.05$). However, the number of cells that infiltrate the bilayered scaffold is significantly reduced at increasing penetration depths (200 and 300 μm) relative to the upper face, Supplementary Figure S4.

4 Discussion

This study addresses a crucial gap in the literature, that previously restricted the development of biomimetic urethral scaffolds, by comprehensively investigating the relationship between urethral tissue mechanics, composition and gross structure. We then utilised these data to develop the first biomimetic urethral scaffold and demonstrate that it's physical properties more accurately mimic the native tissue than the existing gold standard tissue engineered options; SIS and UBM. Urethral tissue exhibited a viscoelastic, pressure stiffening response, during the application of intraluminal pressure (Figure 1). Furthermore, both the elastic and viscous responses of the tissue to extension are free of regional or directional variance (Figure 2). The mechanics of the tissue are shown to correlate with composition, whereby elastin and collagen content correlate with mechanical properties in the low and mid/high pressure ranges, respectively (Figure 3). These data were used to

inform the design of a novel bilayered scaffold which is shown to be more mimetic of human urethral tissue in terms of mechanical properties, composition and gross structure compared to the currently employed tissue engineered gold standards (Figure 5). Furthermore, our biomimetic scaffold demonstrates more uniform cell infiltration compared to SIS and UBM when implanted subcutaneously in a rat model for 1 week (Figure 6).

We perform the first study to comprehensively characterise the physical properties of human urethral tissue. However, the mechanical behaviour characterised in this study has been observed previously in both murine and equine models. Specifically, the mechanical response of murine and equine urethral tissue is viscoelastic and free from regional or directional variance [2,21]. The extension response of formalin-fixed cadaveric urethral tissue previously demonstrated some apparent anisotropy in a limited number of samples [33]. However, formalin fixation dramatically alters the stiffness [13,34–37], failure [34] and directionality [35] of soft tissues, and data derived from such tissue should be regarded with caution. The direct relationship observed between tissue mechanics and composition has not been previously characterised in the urethra. Our data reveal that the relationship is typical of other tubular soft biological tissues such as arteries whereby elastin and collagen are the primary load bearing structures in the low and high pressure ranges, respectively [23]. Although in vivo studies of urethral tissue biomechanics would act as the most appropriate comparison to confirm the ex vivo data generated as part of this study, in vivo studies to date do not provide appropriate comparisons having focused on the female urethra [22,38] or the male prostatic urethra [39,40]. Our results also demonstrate that the mechanical properties of SIS and UBM vary greatly from the native tissue, a finding that is supported by previous reports of SIS and UBM mechanical properties (see Supplementary Table S5). Furthermore, structural characterisation of SIS and UBM confirms that their densely packed laminates are not analogous to the structure of the native tissue and may restrict cellular infiltration, a claim that our *in vivo* data support. Our findings highlight the need for a tissue engineered scaffold that is biomimetic of the native urethral tissue, such as is developed in this study.

Numerous clinical and preclinical studies have investigated acellular collagen based scaffolds for use in urethral tissue engineering [8]. However, studies of elastin based scaffolds for such indications are limited. Xie et al demonstrated that collagen urethral grafts better maintain diameter, while elastin urethral grafts reduce inflammation and fibrosis, therefore suggesting that a scaffold fabricated from both materials would act as an appropriate urethral graft [41]. Bilayered scaffolds with impermeable inner layers and porous outer layers have been employed previously in preclinical studies of urethral grafting [42,43]. However, previous bilayered scaffolds were fabricated from silk fibroin and exhibited mechanical properties equivalent to SIS [44], therefore not replicating the composition or mechanics of the native tissue. The increased cell infiltration observed through the upper face of the bilayered scaffold relative to controls is anticipated to assist in overcoming the poor outcomes observed in long and tubular urethral grafting indications, which have been attributed to the increased endogenous cell infiltration and tissue ingrowth required to bridge the scaffold [9]. Although pre-seeding scaffolds with cells can also improve tissue ingrowth [45–47], the cost of producing such grafts is estimated to be 6 times that of acellular scaffolds with 2–4 weeks of preparation required [48], thereby supporting the need for an effective acellular urethral scaffold.

There are some limitations to this study. Firstly, our samples were obtained from transgender patients who received long term oestrogen hormone treatment prior to surgery. However, there is no evidence to suggest that hormone therapy alters the structure or mechanics of the urethra or surrounding tissues. Additionally, oestrogen is present in the penises of men not engaged in hormone therapy and is believed to play a role in blood vessel regulation [49]. Therefore, the effects of hormone treatment on sample mechanics and composition in this study were not considered. Secondly, samples were frozen at −20°C prior to testing to facilitate transport of the tissue. Although freezing at this temperature has no significant effects on soft tissue mechanics [12,13], freezing without cryoprotective additives can damage cells and may therefore have altered the concentration of smooth and striated muscle cells detected in this study [50]. Future studies wishing to characterise the mechanical properties of human urethral tissue under active smooth muscle contraction should test samples fresh following excision and also include smooth muscle cell activators that trigger a contractile response of the cells [14,15]. Thirdly, work remains to fully characterise the 3D distribution of tissue components, the tissue micro-architecture, and the presentation of tissue-specific bioactive molecules. Such features play an important role in the engraftment and survival of the endogenous cells that infiltrate a urethral scaffold through the presentation of appropriate binding sites and geometrical constraints [51,52]. Future tissue characterisation is therefore required to more comprehensively inform the design of urethral tissue-mimetic scaffolds.

The findings of this study provide the most appropriate data to date for informing the design of urethral grafting material and therefore have considerable implications for the design of tissue engineered urethral scaffolds. Specifically, future urethral scaffolds should be isotropic and can be used to replace both bulbar and penile urethral defects. Furthermore, the correlation between tissue composition and mechanics highlights the important role that structural proteins can play in the design of tissue engineered urethral scaffolds. The positive preliminary findings observed for our biomimetic urethral scaffold warrant additional *in vivo* studies. It is intended to implant this novel scaffold in a rabbit model with an induced stricture [8] for up to 6 months in order to further assess the clinical potential of this promising treatment option. The long term remodelling will be assessed via mechanical characterisation of the explanted graft in addition to staining for smooth muscle cell infiltration, ECM deposition and neo-tissue vascularisation.

5 Conclusion

This study is the first to comprehensively characterise the passive mechanical properties of explanted human male urethra tissue. We then utilised these data to develop a biomimetic urethral scaffold. Urethral tissue exhibits a nonlinear pressure stiffening response that is distinct during static and dynamic loading. Furthermore, both the elastic and viscous responses of the tissue to extension are free from directional and regional variance. Elastin and collagen significantly influence tissue mechanics whereby elastin content correlates positively with compliance in the low pressure range and collagen content correlates positively with overall beta stiffness and incremental modulus in the mid and high pressure ranges. Our novel bilayered scaffold is more mechanically, compositionally and structurally mimetic of the human male urethra than existing gold-standard tissue engineered materials; SIS and UBM. These findings act as a proof-of-concept for a biomimetic off-the-shelf

urethral scaffold and warrant further *in vivo* assessment of the clinical potential of this promising treatment option.

Supplementary Material

Refer to Web version on PubMed Central for supplementary material.

Acknowledgements

The authors would like to acknowledge the work of Dr Emily Ryan and Dr Alan Hibbits at RCSI for their assistance in fabricating bilayered collagen-elastin scaffolds, the work of Prerak Gupta of the Indian Institute of Technology Guwahati for his assistance in acquiring SEM images, and Dr John Mulvihill for providing the chemicals required to prepare tissue samples for SEM analysis. The collagen used in this study was supplied under a Materials Transfer Agreement by Integra Life Sciences. The authors would like to thank Cook Medical Ltd. and ACell Inc. for their kind donation of SIS and UBM, respectively. Figures 1 and 6 were partially created with BioRender.com.

8 Funding sources

This work was funded by the European Union's Horizon 2020 research and innovation program under the Marie Sklodowska-Curie grant agreement No 708867 awarded to EC, the Competitive Medical Research Fund, University of Pittsburgh awarded to JW and the National Institute of Health under grant agreement No R01HL130077 awarded to DV.

10 Data availability

The raw and processed data required to reproduce the findings related to the characterisation of human male urethra tissue are available at Zenodo.org as Dataset for 'Mechanical, compositional and morphological characterisation of the human male urethra for the development of a biomimetic tissue engineered urethral scaffold'. The raw and processed data required to reproduce the findings related to the development of the bilayered urethral scaffold will be made available upon request to the lead author (eoghanmcunnane@gmail.com).

List of Abbreviations:

UBM	urinary bladder matrix
VVG	Verhoeff-van Gieson
SIS	small Intestinal submucosa
MTC	Mason's trichrome
ddH_2O	deionised distilled water
SMA	smooth muscle actin

12 References

1. Brading AF Physiological Society Symposium : The Physiology and Pathophysiology of the Lower Urinary Tract: The Physiology of the Mammalian Urinary Outflow Tract. Exp. Physiol 1999, 84, 215–221. [PubMed: 10081719]

2. Prantil RL, Jankowski RJ, Kaiho Y, de Groat WC, Chancellor MB, Yoshimura N & Vorp DA Ex Vivo Biomechanical Properties of the Female Urethra in a Rat Model of Birth Trauma. Am. J. Physiol. - Ren. Physiol 2007, 292, F1229–F1237.

3. Orabi H, Bouhout S, Morissette A, Rousseau A, Chabaud S & Bolduc S Tissue Engineering of Urinary Bladder and Urethra: Advances from Bench to Patients. Sci. World J 2013, 2013,.

4. Santucci RA, Joyce GF & Wise M Male Urethral Stricture Disease. J. Urol 2007, 177, 1667–1674. [PubMed: 17437780]

5. Harris CR, Osterberg EC, Sanford T, Alwaal A, Gaither TW, McAninch JW, McCulloch CE & Breyer BN National Variation in Urethroplasty Cost and Predictors of Extreme Cost: A Cost Analysis With Policy Implications. Urology. 2016, 94, 246–254. [PubMed: 27107626]

6. Blaschko SD, Harris CR, Zaid UB, Gaither T, Chu C, Alwaal A, McAninch JW, McCulloch CE & Breyer BN Trends, Utilization, and Immediate Perioperative Complications of Urethroplasty in the United States: Data From the National Inpatient Sample 2000–2010. Urology. 2015, 85, 1190–1194. [PubMed: 25746579]

7. Browne BM & Vanni AJ Use of Alternative Techniques and Grafts in Urethroplasty. Urol. Clin. NA 2017, 44, 127–140.

8. Versteegden LRM, de Jonge PKJD, IntHout J, van Kuppevelt TH, Oosterwijk E, Feitz WFJ, de Vries RBM & Daamen WF Tissue Engineering of the Urethra: A Systematic Review and Meta-Analysis of Preclinical and Clinical Studies [Figure Presented]. Eur. Urol 2017, 72, 594–606. [PubMed: 28385451]

9. Davis NF, Cunnane EM, O'Brien FJ, Mulvihill JJ & Walsh MT Tissue Engineered Extracellular Matrices (ECMs) in Urology: Evolution and Future Directions. Surgeon. 2017, doi:10.1016/j.surge.2017.07.002.

10. Feng C, Xu Y, Fu Q, Zhu W, Cui L & Chen J Evaluation of the Biocompatibility and Mechanical Properties of Naturally Derived and Synthetic Scaffolds for Urethral Reconstruction. 2010, 1–8 doi:10.1002/jbm.a.32729.

11. Rohman G, Pettit JJ, Isaure F, Cameron NR & Southgate J Influence of the Physical Properties of Two-Dimensional Polyester Substrates on the Growth of Normal Human Urothelial and Urinary Smooth Muscle Cells in Vitro. Biomaterials. 2007, 28, 2264–2274. [PubMed: 17296219]

12. O'Leary SA, Doyle BJ & McGloughlin TM The Impact of Long Term Freezing on the Mechanical Properties of Porcine Aortic Tissue. J. Mech. Behav. Biomed. Mater 2014, 37, 165–173. [PubMed: 24922621]

13. Ebenstein DM, Coughlin D, Chapman J, Li C & Pruitt L a. Nanomechanical Properties of Calcification, Fibrous Tissue, and Hematoma from Atherosclerotic Plaques. J. Biomed. Mater. Res. A 2009, 91, 1028–37. [PubMed: 19107789]

14. Jankowski RJ, Prantil RL, Chancellor MB, de Groat WC, Huard J & Vorp D a. Biomechanical Characterization of the Urethral Musculature. Am. J. Physiol. Renal Physiol 2006, 290, F1127–34. [PubMed: 16368741]

15. Jankowski RJ, Prantil RL, Fraser MO, Chancellor MB, De Groat WC, Huard J & Vorp D a. Development of an Experimental System for the Study of Urethral Biomechanical Function. Am. J. Physiol. Renal Physiol 2004, 286, F225–32. [PubMed: 14506075]

16. Schmidt F, Yoshimura Y, Shin PY & Constantinou CE Comparative Urodynamic Patterns of Bladder Pressure, Contractility and Urine Flow in Man and Rat during Micturition. APMIS. Suppl 2003, 111, 39–44.

17. Magnan M, Lévesque P, Gauvin R, Dubé J, Barrieras D, El-Hakim A & Bolduc S Tissue Engineering of a Genitourinary Tubular Tissue Graft Resistant to Suturing and High Internal Pressures. Tissue Eng. Part A 2009, 15, 197–202. [PubMed: 18759664]

18. Schindelin J, Rueden CT, Hiner MC & Eliceiri KW The ImageJ Ecosystem: An Open Platform for Biomedical Image Analysis. Mol. Reprod. Dev. 2015, 529, 518–529.

19. Mulvihill JJ & Walsh MT On the Mechanical Behaviour of Carotid Artery Plaques: The Influence of Curve-Fitting Experimental Data on Numerical Model Results. Biomech. Model. Mechanobiol 2013, 12, 975–85. [PubMed: 23192833]

20. Hollenstein M, Ehret AE, Itskov M & Mazza E A Novel Experimental Procedure Based on Pure Shear Testing of Dermatome-Cut Samples Applied to Porcine Skin. Biomech. Model. Mechanobiol 2011, 10, 651–661. [PubMed: 21069417]
21. Natali AN, Carniel EL, Frigo A, Pavan PG, Todros S, Pachera P, Fontanella CG, Rubini A, Cavicchioli L, Avital Y & De Benedictis GM Experimental Investigation of the Biomechanics of Urethral Tissues and Structures. Exp. Physiol 2016, 101, 641–656. [PubMed: 26864993]
22. Thind P An Analysis of Urethral Viscoelasticity with Particular Reference to the Sphincter Function in Healthy Women. International Urogynecology Journal And Pelvic Floor Dysfunction. 1995, vol. 6 209–228.
23. Holzapfel GA Biomechanics of Soft Tissue. (Academic Press, 2000).
24. Skrzypek JJ & Ganczarski AW Engineering Materials: Mechanics of Anisotropic Materials. (2015). doi:10.1007/978-3-319-17160-9.
25. Bauman TM, Nicholson TM, Abler LL, Eliceiri KW, Huang W, Vezina CM & Ricke WA Characterization of Fibrillar Collagens and Extracellular Matrix of Glandular Benign Prostatic Hyperplasia Nodules. PLoS One. 2014, 9, 1–9.
26. Cunnane EM, Barrett HE, Kavanagh EG, Mongrain R & Walsh MT The Influence of Composition and Location on the Toughness of Human Atherosclerotic Femoral Plaque Tissue. Acta Biomater. 2016, 31,.
27. Ryan AJ & O'Brien FJ Insoluble Elastin Reduces Collagen Scaffold Stiffness, Improves Viscoelastic Properties, and Induces a Contractile Phenotype in Smooth Muscle Cells. Biomaterials. 2015, 73, 296–307. [PubMed: 26431909]
28. O'Brien FJ, Harley BA, Yannas IV & Gibson L Influence of Freezing Rate on Pore Structure in Freeze-Dried Collagen-GAG Scaffolds. Biomaterials. 2004, 25, 1077–1086. [PubMed: 14615173]
29. Haugh MG, Jaasma MJ & O'Brien FJ The Effect of Dehydrothermal Treatment on the Mechanical and Structural Properties of Collagen-GAG Scaffolds. J. Biomed. Mater. Res. - Part A 2009, 89, 363–369.
30. Roh JD, Sawh-Martinez R, Brennan MP, Jay SM, Devine L, Rao DA, Yi T, Mirensky TL, Nalbandian A, Udelsman B, Hibino N, Shinoka T, Saltzman WM, Snyder E, Kyriakides TR, Pober JS & Breuer CK Tissue-Engineered Vascular Grafts Transform into Mature Blood Vessels via an Inflammation-Mediated Process of Vascular Remodeling. Proc. Natl. Acad. Sci 2010, 107, 4669–4674. [PubMed: 20207947]
31. Cunnane EM, Mulvihill JJE, Barrett HE, Hennessy MM, Kavanagh EG & Walsh MT Mechanical Properties and Composition of Carotid and Femoral Atherosclerotic Plaques: A Comparative Study. J. Biomech 2016, 49,. [PubMed: 27988036]
32. Gupta P, Lorentz KL, Haskett DG, Cunnane EM, Ramaswamy AK, Weinbaum JS, Vorp DA & Mandal BB Bioresorbable Silk Grafts for Small Diameter Vascular Tissue Engineering Applications: In Vitro and in Vivo Functional Analysis. Acta Biomater. 2020, doi:10.1016/j.actbio.2020.01.020.
33. Masri C, Chagnon G, Favier D, Sartelet H & Girard E Experimental Characterization and Constitutive Modeling of the Biomechanical Behavior of Male Human Urethral Tissues Validated by Histological Observations. Biomech. Model. Mechanobiol 2018, 17, 939–950. [PubMed: 29380159]
34. Hohmann E, Keough N, Glatt V, Tetsworth K, Putz R & Imhoff A The Mechanical Properties of Fresh versus Fresh/Frozen and Preserved (Thiel and Formalin) Long Head of Biceps Tendons: A Cadaveric Investigation. Ann. Anat 2019, 221, 186–191. [PubMed: 29879483]
35. Rouleau L, Tremblay D, Cartier R, Mongrain R & Leask RL Regional Variations in Canine Descending Aortic Tissue Mechanical Properties Change with Formalin Fixation. Cardiovasc. Pathol 2012, 21, 390–397. [PubMed: 22300500]
36. Xu L, Chen J, Yin M, Glaser KJ, Chen Q, Woodrum DA & Ehman RL Assessment of Stiffness Changes in the Ex Vivo Porcine Aortic Wall Using Magnetic Resonance Elastography. Magn. Reson. Imaging 2012, 30, 122–127. [PubMed: 22055848]
37. Park J, Siegel R & Demer L Effect of Calcification and Formalin Fixation on in Vitro Distensibility of Human Femoral Arteries. Am. Heart J 1993,.

38. Lose G & Colstrup H Mechanical Properties of the Urethra in Healthy and Stress Incontinent Females: Dynamic Measurements in the Resting Urethra. J Urol. 1990, 144, 1258–1262. [PubMed: 2231912]
39. Aagaard M, Klarskov N, Sønksen J, Bagi P, Colstrup H & Lose G Urethral Pressure Reflectometry; A Novel Technique for Simultaneous Recording of Pressure and Cross-Sectional Area: A Study of Feasibility in the Prostatic Urethra. BJU Int. 2012, 110, 1178–1183. [PubMed: 22416900]
40. Bagi P, Bøtker-Rasmussen I & Kristensen JK Pressure/Cross-Sectional Area Relations in the Proximal Urethra of Healthy Males: The Time Dependent Pressure Response Following Forced Dilation. Part IV: Results in Healthy Volunteers. Urol. Res 2002, 30, 9–14. [PubMed: 11942330]
41. Xie H, Campbell CE, Shaffer BS & Gregory KW Different Outcomes in Urethral Reconstruction Using Elastin and Collagen Patches and Conduits in Rabbits. J. Biomed. Mater. Res. - Part B Appl. Biomater 2007, 81, 269–273.
42. Algarrahi K, Affas S, Sack BS, Yang X, Costa K, Seager C, Estrada CR & Mauney JR Repair of Injured Urethras with Silk Fibroin Scaffolds in a Rabbit Model of Onlay Urethroplasty. J. Surg. Res 2018, 229, 192–199. [PubMed: 29936989]
43. Chung YG, Tu D, Franck D, Gil ES, Algarrahi K, Adam RM, Kaplan DL, Estrada CR & Mauney JR Acellular Bi-Layer Silk Fibroin Scaffolds Support Tissue Regeneration in a Rabbit Model of Onlay Urethroplasty. PLoS One. 2014, 9, 1–7.
44. Seth A, Chung YG, Gil ES, Tu D, Franck D, Di Vizio D, Adam RM, Kaplan DL, Estrada CR & Mauney JR The Performance of Silk Scaffolds in a Rat Model of Augmentation Cystoplasty. Biomaterials. 2013, 34, 4758–4765. [PubMed: 23545287]
45. Raya-Rivera A, Esquiliano DR, Yoo JJ, Lopez-Bayghen E, Soker S & Atala A Tissue-Engineered Autologous Urethras for Patients Who Need Reconstruction: An Observational Study. Lancet. 2011, 377, 1175–1182. [PubMed: 21388673]
46. Engel O, Ram-Liebig G, Reiß P, Schwaiger B, Pfalzgraf D, Dahlem R & Fisch M 15 Tissue - Engineered Buccal Mucosa Urethroplasty. Outcome of Our First 10 Patients. J. Urol 2012, 187, e6.
47. Ram-Liebig G, Bednarz J, Stuerzebecher B, Fahlenkamp D, Barbagli G, Romano G, Balsmeyer U, Spiegeler ME, Liebig S & Knispel H Regulatory Challenges for Autologous Tissue Engineered Products on Their Way from Bench to Bedside in Europe. Adv. Drug Deliv. Rev 2015, 82, 181–191. [PubMed: 25446139]
48. Mangera A & Chapple CR Tissue Engineering in Urethral Reconstruction—an Update. Asian J. Androl 2012, 89–92 doi:10.1038/aja.2012.91. [PubMed: 23042444]
49. Dietrich W, Haitel a, Huber JC & Reiter WJ Expression of Estrogen Receptors in Human Corpus Cavernosum and Male Urethra. J Histochem Cytochem. 2004, 52, 355–360. [PubMed: 14966202]
50. Müller-Schweinitzer E Cryopreservation of Vascular Tissues. Organogenesis. 2009, 5, 97–104. [PubMed: 20046671]
51. Werner M, Kurniawan NA & Bouten CVC Cellular Geometry Sensing at Different Length Scales and Its Implications for Scaffold Design. Materials (Basel). 2020, 13, 1–18.
52. Pederzoli F, Joice G, Salonia A, Bivalacqua TJ & Sopko NA Regenerative and Engineered Options for Urethroplasty. Nat. Rev. Urol 2019, 16, 453–464. [PubMed: 31171866]

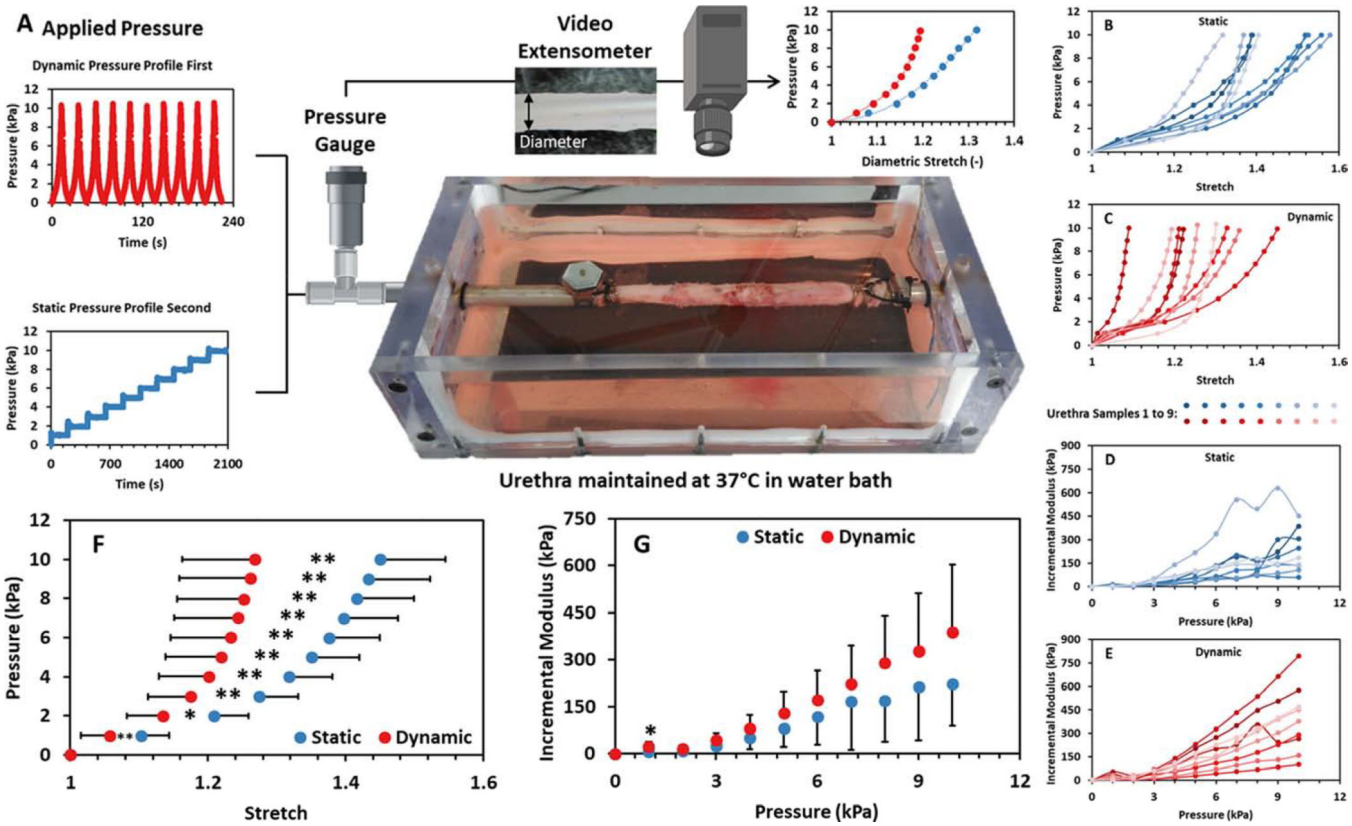

Figure 1:

A) Schematic of the experimental apparatus used to perform pressure-diameter testing of the human urethral samples characterised in this study. Intraluminal pressure was applied as either a dynamic or static pressure profile. The corresponding changes in pressure and diameter were monitored using a pressure transducer and video extensometer respectively to generate diametric stretch-pressure data. **B** to **G)** Mechanical results obtained from pressure-diameter testing of intact human male urethras (n = 9). **B** and **C)** The diametric stretch response of samples to static and dynamic loading, respectively. **D** and **E)** The incremental modulus exhibited by the samples during static and dynamic loading, respectively. **F)** The mean diametric stretch response of the samples under static and dynamic loading, and **G)** the corresponding mean incremental modulus. Error bars depict 1 standard deviation from the mean. * indicates significance at $p < 0.05$ and ** indicates significance at $p < 0.01$.

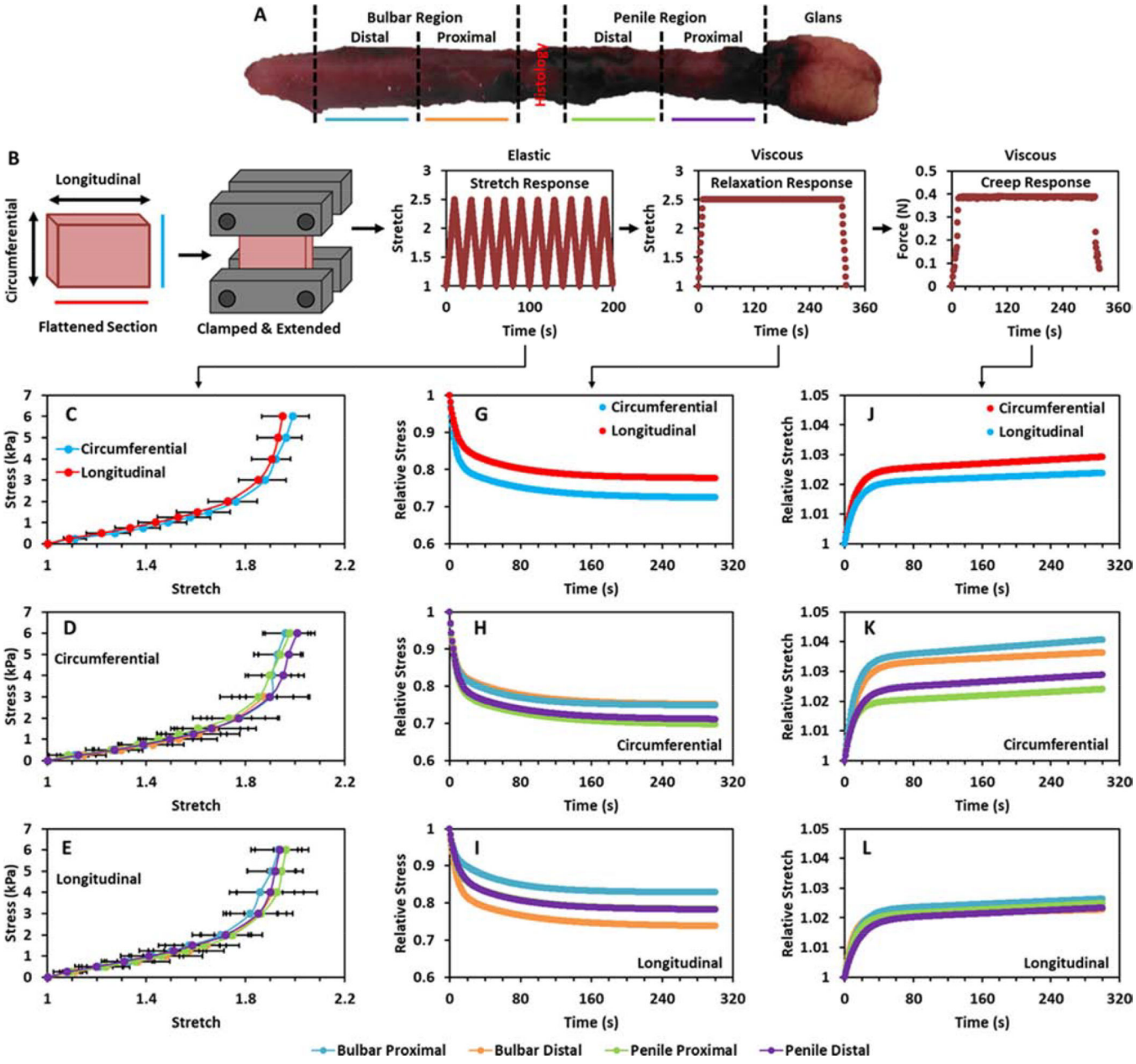

Figure 2:

A) Human urethra sample and the regions characterised. **B)** Method of sectioning and extending samples during planar tension testing and the manner of loading applied to the tissue. **C)** Direction average response of the tissue to extension in the circumferential and longitudinal directions. **D** and **E)** Region averaged response of the proximal bulbar, distal bulbar, proximal penile and distal penile tissue to planar tension testing in the circumferential **D)** and longitudinal **E)** directions. **G)** Direction average response of the tissue to sustained stretch in the circumferential and longitudinal directions. **H** and **I)** Region average response of the tissue to sustained stretch in the circumferential **H)** and longitudinal **I)** directions. **J)** Direction average response of the tissue to sustained stress in the

circumferential and longitudinal directions. **K** and **L)** Region average response of the tissue to sustained stress in the circumferential **K)** and longitudinal **L)** directions.

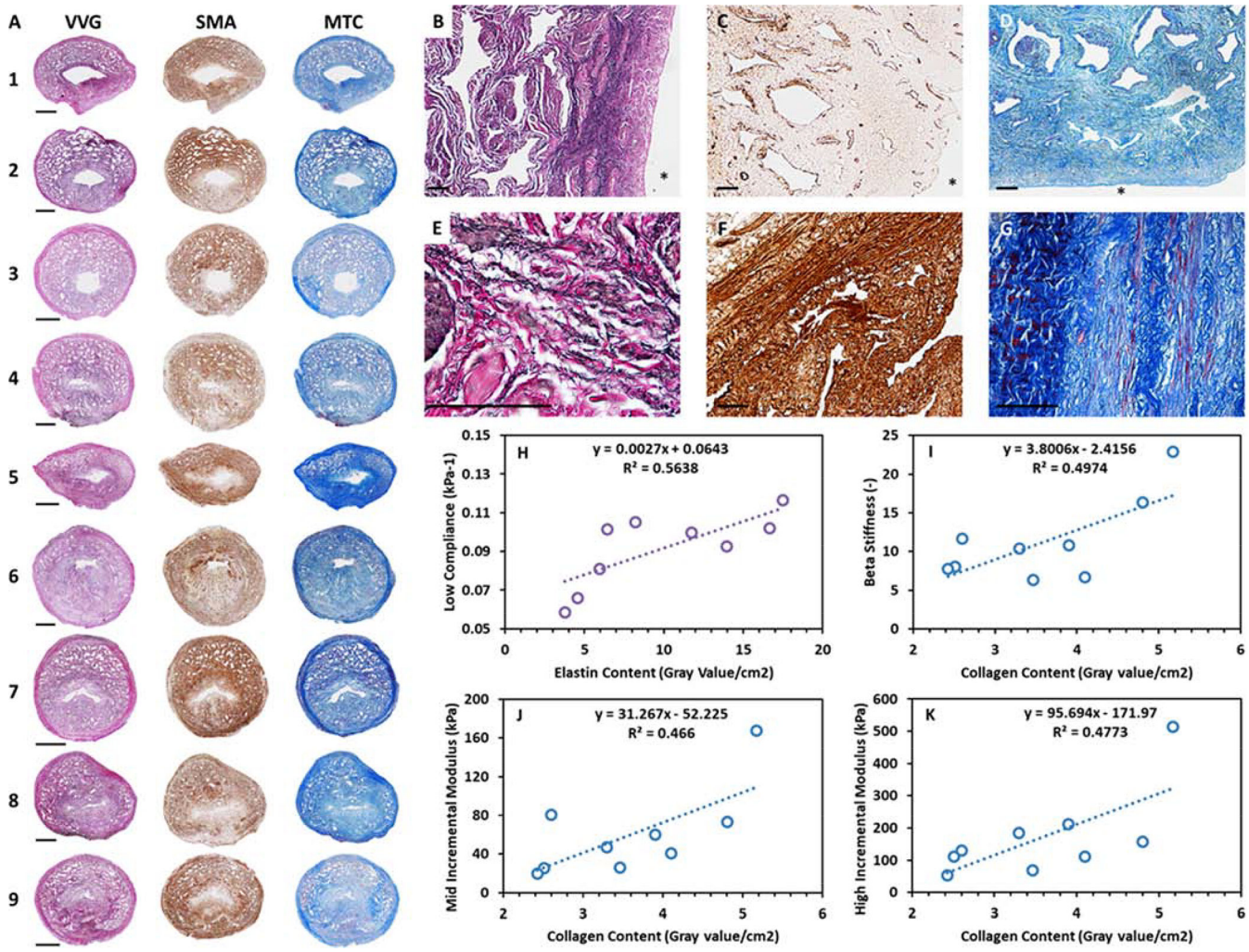

Figure 3:

A) Verhoeff-Van Gieson (VVG), smooth muscle actin (SMA) and Mason's trichrome (MTC) staining of all samples characterised in this study to identify elastin (black), muscle (brown) and collagen (blue) content respectively. Scale bars depict 2 mm. **B** to **D)** Magnified elastin, muscle and collagen stains depicting the inner non-porous submucosa layer adjacent to the lumen and the outer porous corpus spongiosum layer of samples 1, 2 and 8. Scale bars depict 100 μm and * depicts the lumen. **E** to **G)** Magnified elastin, muscle and collagen stains from sample 7. Scale bars depict 100 μm **H)** Significant positive relationship between elastin content and compliance in the low pressure range. **I** to **K)** Significant positive relationships between collagen content and Beta stiffness and incremental modulus in the mid and high pressure regions.

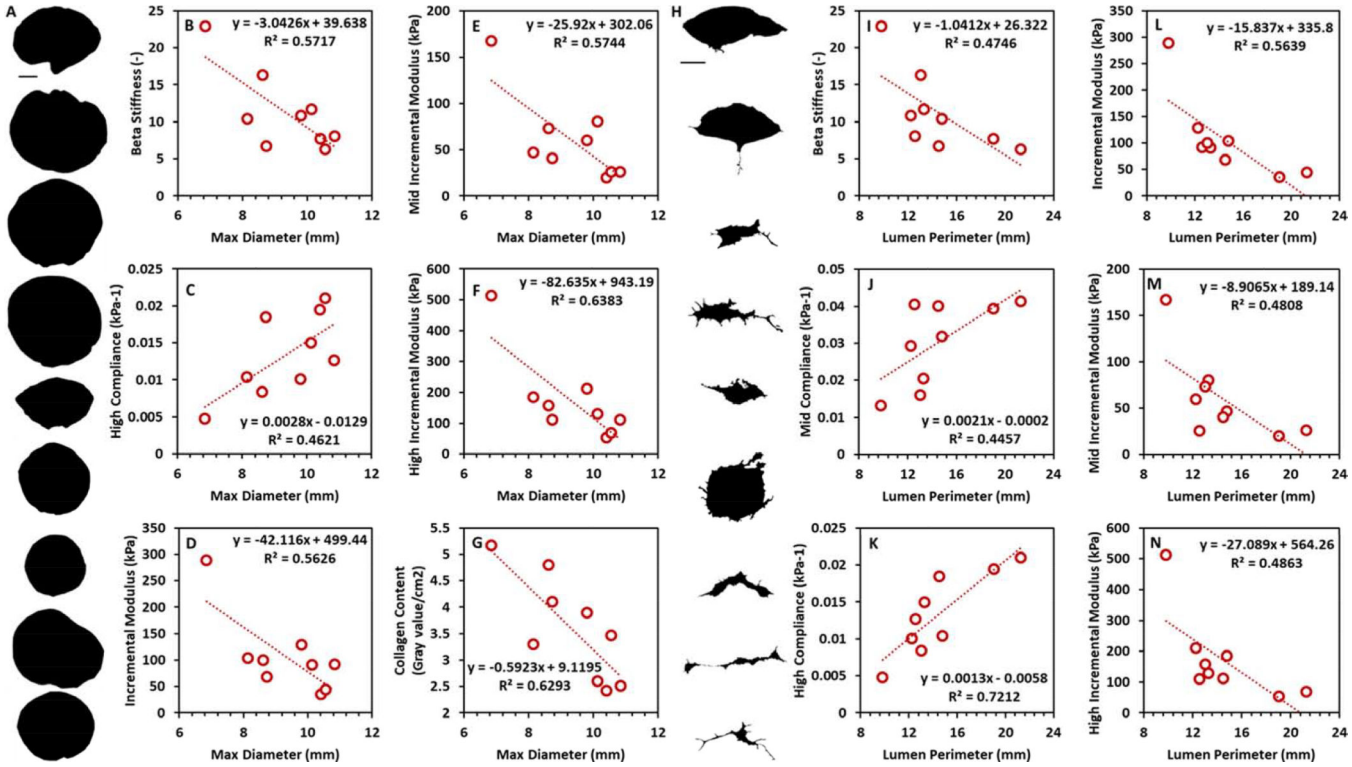

Figure 4:

A) Cross sectional profile of urethra samples characterised in this study. Scale bar depicts 2 mm. **B** to **G)** Significant relationships identified between max diameter and **(B)** Beta stiffness, **(C)** compliance in the high pressure range, **(D)** overall incremental modulus, incremental modulus in the **(E)** mid and **(F)** high pressure ranges and **(G)** collagen content. **H)** Lumen profile of urethra samples characterised in this study. Scale bar depicts 1 mm. **I to N)** Significant relationships identified between perimeter and **(I)** Beta stiffness, compliance in the **(J)** mid and **(K)** high pressure ranges, **(L)** overall incremental modulus and incremental modulus in the **(M)** mid and **(N)** high pressure regions.

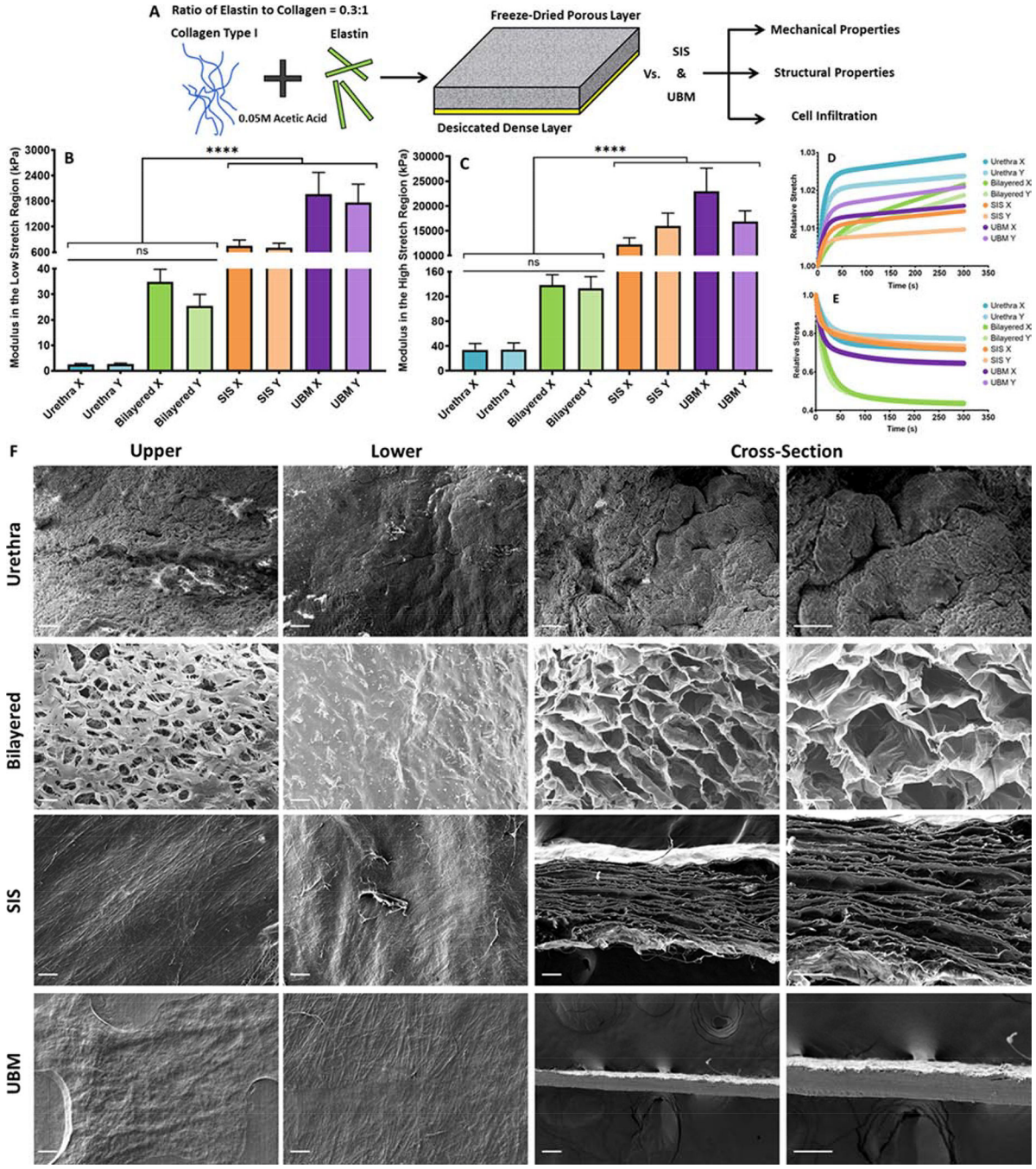

Figure 5:

A) Method of fabricating and characterising the collagen-elastin bilayered scaffolds, UBM and SIS. **B)** The modulus of each tissue engineered material in the low stretch region compared to the native urethral tissue. **C)** The modulus of each tissue engineered material in the high stretch region compared to the native urethral tissue. **D)** Creep behaviour of each tissue engineered material compared to the native urethral tissue. **E)** Stress relaxation behaviour of each tissue engineered material compared to the native urethral tissue. **F)** Micrographs of the upper face, lower face and cross-section of the native urethra and each

tissue engineered material. Scale bars depict 100 μm. Error bars depict 1 standard deviation from the mean. **** indicates significance at $p \leq 0.0001$.

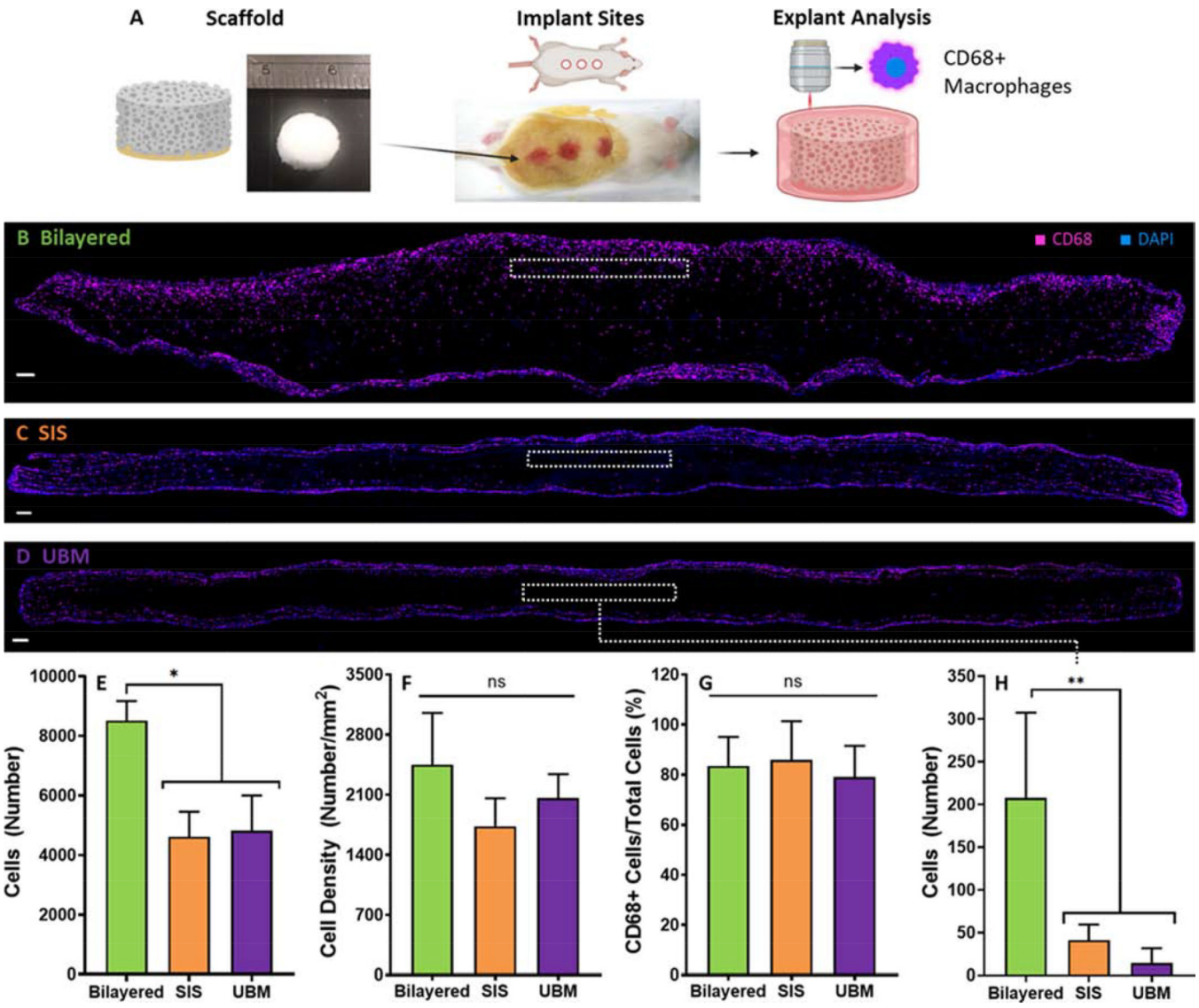

Figure 6:

A Method of implanting the bilayered scaffold and analysing the explanted tissue. **B** to **D)** Representative immunofluorescecnt images of the explanted scaffolds. Blue indicates positive DAPI staining and magenta indicates positive CD68 staining. **B)** Explanted bilayered scaffold **C)** Explanted SIS scaffold. **D)** Explanted UBM scaffold. **E)** The number of cells that infiltrated each scaffold type following subcutaneous implantation in a rat model. **F)** The cellular density of each scaffold type. **G)** The ratio of CD68+ cells to the total number of cells present in the explants. **H)** The number of cells that infiltrate a $0.1mm^2$ area of interest at a distance of 100 μm from the scaffolds upper face (depicted by the inset dashed line boxes in **B** to **D)**. Error bars depict 1 standard deviation from the mean. Scale bars depict 100 μm. * indicates significance at $p < 0.05$.

Table 1:

Beta stiffness, compliance and incremental modulus of the samples under static and dynamic loading. P values refer to the statistical significance of differences observed between the samples during the static and dynamic loading.

		Compliance (kPa^{-1})			Incremental Modulus (kPa)			
	Stiffness (−)	**Low**	**Mid**	**High**	**Overall**	**Low**	**Mid**	**High**
Static	11.262 (5.734)	0.093 (0.02)	0.03 (0.012)	0.014 (0.006)	103.085 (79.514)	5.884 (3.716)	59.899 (48.757)	166.123 (146.566)
Dynamic	20.204 (10.341)	0.06 (0.023)	0.0175 (0.011)	0.008 (0.005)	157.878 (87.641)	16.252 (11.817)	95.626 (58.272)	264.718 (155.763)
P value	0.031*	0.006**	0.011*	0.031*	0.094	0.04*	0.113	0.094

Table 2:

Mean values (SD) of the parameters defining the relaxation response of the urethral tissue to sustained extension. Tissue was tested in both the circumferential (circ) and longitudinal (long) directions. The tissue was also divided into the different regions of the urethra. Significant differences were not identified between the responses in terms of test direction or region of the urethra.

Location	Direction	$\gamma 1$	$\gamma 2$	$\tau 1$	$\tau 2$
Overall	**Circ**	0.251 (0.069)	0.067 (0.033)	20.491 (6.094)	449.572 (57.139)
	Long	0.201 (0.067)	0.055 (0.020)	19.625 (6.363)	475.968 (59.610)
Bulbar Proximal	**Circ**	0.229 (0.097)	0.057 (0.025)	20.854 (6.244)	443.906 (17.926)
	Long	0.223 (0.088)	0.056 (0.029)	19.366 (8.668)	486.060 (56.345)
Bulbar Distal	**Circ**	0.227 (0.077)	0.076 (0.043)	17.294 (3.505)	473.346 (23.071)
	Long	0.163 (0.054)	0.043 (0.001)	17.682 (6.281)	481.790 (86.613)
Penile Proximal	**Circ**	0.282 (0.039)	0.060 (0.025)	22.631 (5.895)	462.357 (37.485)
	Long	0.199 (0.057)	0.053 (0.015)	17.862 (4.847)	459.746 (78.421)
Penile Distal	**Circ**	0.255 (0.052)	0.083 (0.041)	19.273 (7.121)	429.676 (101.479)
	Long	0.198 (0.059)	0.061 (0.016)	22.509 (4.859)	479.509 (27.306)

Table 3:

Mean values (SD) of the parameters defining the creep response of the urethral tissue to sustained force. Tissue was tested in both the circumferential (circ) and longitudinal (long) directions. The tissue was also divided into the regions of the urethra. Significant differences were not identified between the responses in terms of test direction or region of the urethra.

Location	Direction	R1	R2	η1	η2
Overall	**Circ**	3.011 (2.921)	16.481 (7.659)	182331.214 (78362.093)	194.138 (172.033)
	Long	2.661 (2.103)	19.665 (11.426)	230899.313 (153152.032)	254.618 (203.740)
Bulbar Proximal	**Circ**	2.583 (1.256)	12.489 (6.818)	180006.404 (84459.191)	169.903 (217.637)
	Long	1.752 (1.283)	19.266 (11.363)	273631.139 (247877.549)	190.602 (187.650)
Bulbar Distal	**Circ**	3.377 (1.649)	11.707 (4.768)	155210.870 (58735.492)	139.527 (139.973)
	Long	2.198 (1.729)	17.754 (20.458)	173777.436 (63340.659)	244.175 (160.605)
Penile Proximal	**Circ**	2.732 (1.432)	20.746 (8.897)	172955.126 (89930.266)	203.444 (156.406)
	Long	3.375 (2.924)	19.765 (10.322)	220039.735 (113887.363)	244.600 (184.001)
Penile Distal	**Circ**	3.561 (5.150)	16.967 (5.630)	205083.652 (73755.998)	225.353 (180.776)
	Long	3.062 (1.864)	20.815 (9.668)	224414.567 (90412.799)	333.292 (255.304)

Table 4:

Area (mm^2) and percentage area (%) occupied in each sample by the tissue matrix components characterised in this study. Colour intensity per tissue area of the tissue matrix components characterised in this study for each sample.

	Area (mm^2)			Area Percentage (%)			Ratio	Colour Intensity/Area (Gray value/cm^2)		
No.	**Collagen**	**Elastin**	**Muscle**	**Collagen**	**Elastin**	**Muscle**	**Elastin:Collagen**	**Collagen**	**Elastin**	**Muscle**
1	40.02	16.78	16.63	54.5	22.85	22.65	0.42	3.9	5.94	4.93
2	57.68	22.08	25.59	54.75	20.96	24.29	0.38	2.51	4.55	3.15
3	43.25	6.31	14.25	67.78	9.88	22.34	0.15	3.3	17.5	5.94
4	65.57	13.55	19.19	66.7	13.78	19.52	0.21	2.43	8.2	4.63
5	30.72	7.88	12.74	59.84	15.34	24.81	0.26	4.1	13.96	6.8
6	51.13	6.95	15.06	69.91	9.51	20.59	0.14	3.46	16.66	5.41
7	26.71	8.72	20.94	47.38	15.47	37.15	0.33	5.17	11.75	4.18
8	57.69	24.54	18.6	57.22	24.34	18.45	0.43	2.6	3.76	4.64
9	37.2	14.91	17.93	53.11	21.29	25.61	0.4	4.8	6.44	4.66
Avg	45.55	13.52	17.88	59.02	17.05	23.93	0.3	3.59	9.86	4.93
SD	12.5	6.3	3.65	7.21	5.21	5.2	0.11	0.94	4.95	0.98